Time-Resolved Small-Angle X-ray Scattering Studies on the Crystallization of Poly(ethylene terephthalate)

Chang Hyung Lee, Hiromu Saito, and Takashi Inoue*

Department of Organic and Polymeric Materials, Tokyo Institute of Technology, Ookayama, Meguro-ku, Tokyo 152, Japan

Shuichi Nojima

JAIST, Asahidai, Tatsunokuchi, Ishikawa 923-12, Japan

Received December 12, 1995; Revised Manuscript Received July 29, 1996[⊗]

ABSTRACT: We investigated the isothermal crystallization of poly(ethylene terephthalate) by time-resolved small-angle X-ray scattering (SAXS) using synchrotron radiation. At the early stage, the SAXS intensity decreased monotonously with scattering angle (stage I). Then the SAXS profile showed a peak and the peak position progressively moved to a wider angle with crystallization time (stage II). Finally, the peak intensity rapidly increased, keeping the peak angle constant (stage III). The Guinier and the correlation function analyses suggested that crystalline domains of several tens of nanometers in diameter appear and they consist of the highly disordered lamellae (stage I). In stage II, the crystalline domains grow up to the larger domains in which stacking of lamellae is achieved by insertion of newly formed lamellae between the preformed lamellae. Then they develop to yield the spherulites by attaining a higher ordering of the lamellar stacks in stage III.

Introduction

The spherulite is a crystal aggregate with spherical symmetry. Such aggregation arises by radial growth of the crystal from a common center. The spherulitic growth is believed to occur in two ways.[1,2] In growth mechanism A, a central nucleating entity initiates crystal growth in all directions. In growth mechanism B, the spherulite develops from one single crystal through essentially unidirectional growth and the spherical shape is attained through continuous branching and fanning via the intermediate stage of sheaves.[2]

In a previous paper,[3] we investigated the crystallization mechanism in poly(ethylene terephthalate) (PET) by time-resolved light scattering under H_V (cross-polarized) and V_V (parallel-polarized) optical alignments using a highly sensitive CCD (charge-coupled device) camera system. The proposed mechanism was somewhat different from both mechanisms A and B: a highly disordered crystalline domain (ca. 0.3 μm) with low crystallinity appears at early stages and it grows, increasing the ordering and providing the spherical symmetry at later stages. However, light scattering is less informative for fine morphologies smaller than submicrometer so that, for a better understanding of morphology development at the nanometer level at the early stages, one needs the time-resolved small-angle X-ray scattering (SAXS) studies.

In this paper, we carried out the time-resolved SAXS studies on the isothermal crystallization of PET for real-time observation at the lamellar level. The results will be combined with those by light scattering to discuss the development of crystalline morphology ranging from the lamellar level to a few micrometers.

Experimental Section

PET was supplied by Toyobo Co., Ltd. ($M_w = 6 \times 10^3$, $M_n = 3 \times 10^3$). PET pellets were dried under vacuum (10^{-4} mmHg) at 160 °C for 16 h to remove water before melt-pressing. The pellets were compression-molded between metal plates at 290 °C for 4 min. The molded specimen was quickly quenched in a water bath to obtain an amorphous specimen. The specimen was then cut into thin strips (7 mm × 5 mm × 1 mm) and again dried under vacuum at room temperature for 24 h. Then this specimen was used for time-resolved SAXS.

The melt-quenched amorphous specimen was placed in a chamber set at room temperature and then transferred quickly into a hot chamber set at a desired crystallization temperature T_c. The isothermal crystallization at T_c was investigated by the time-resolved SAXS. The X-ray beam was from synchrotron radiation; beam line BL-10C at National Laboratory for High Energy Physics, Tsukuba, Japan (Photon Factory).[4]

The storage ring was operated at an energy level of 2.5 GeV with the ring current of 250−300 mA. The SAXS employs a point focusing optics with a double flat monochromator followed by a bent cylindrical mirror. The incident beam intensity of 0.1488 nm wavelength was monitored by an ionization chamber for the correction of a minor decrease of the primary beam intensity during the measurement. The scattered intensity was detected with a one-dimensional position sensitive proportional counter (PSPC) with 512 channels, and the distance between the sample and the PSPC was about 2 m. The geometry was checked by a chicken tendon collagen, which gives a set of sharp diffractions corresponding to a Bragg spacing of 65.3 nm.

The scattering intensity, I, was corrected for background scattering after a smoothing procedure. The smoothing of the experimental scattering data was performed by a binomial smooth. Then the scattering intensity by thermal fluctuations was subtracted from the SAXS profile $I(q)$ by evaluating the slope of $I(q)q^4$ versus q^4 plots[5] at wide scattering vectors q, where q is $(4\pi/\lambda)$ sin θ, λ and θ being the wavelength and scattering angle, respectively. In order to obtain the invariant Q_{SAXS} (eq 1) and the correlation function of $\gamma_1(r)$ (eq 2), the value of the intercept of an $I(q)q^4$ versus q^4 plot K was used to extrapolate the intensity ($=Kq^{-4}$) to $q = \infty$, whereas $Iq^{-1/2}$ versus q^2 was used to extrapolate the intensity at a small q region to $q = 0$. The correction for smearing effect by the finite cross section of the incident beam was not necessary for the optics of SAXS with point focusing.

Results and Discussion

Figure 1 shows the change in SAXS profile during isothermal crystallization at $T_c = 110$ °C. The time evolution of the scattering profile can be divided into

* To whom correspondence should be addressed.

[⊗] Abstract published in *Advance ACS Abstracts,* October 1, 1996.

S0024-9297(95)01828-6 CCC: $12.00

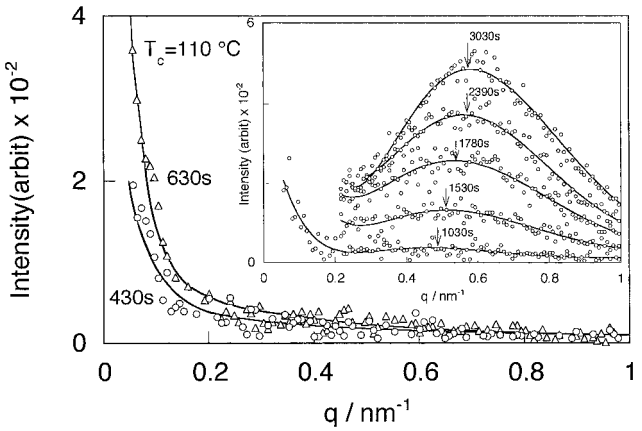

Figure 1. SAXS profiles at various crystallization times.

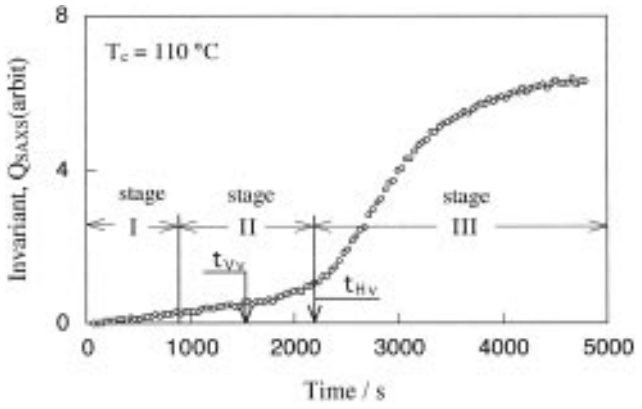

Figure 2. Time variation of the invariant Q_{SAXS}. t_{V_V} and t_{H_V} are the onset times of light scattering invariants at V_V and H_V modes, respectively.

three stages as follows. At $t = 430-630$ s, the scattering intensity decreases monotonously with q (stage I). Then, the scattering profile shows a peak at about $q = 0.5$ nm^{-1}, and the peak position gradually shifts to larger scattering vector with time ($t = 1030-1780$ s; stage II). The change is accompanied with an increase in the intensity. Finally, the scattering intensity increases with time, keeping the peak position constant ($t = 2390-3030$s; stage III).

To discuss the crystallization kinetics, it is convenient to employ the integrated scattering intensity, i.e., the invariant Q_{SAXS} defined by[6]

$$Q_{SAXS} = \int_0^\infty q^2 I(q)\, dq \qquad (1)$$

The time variation of Q_{SAXS} at $T_c = 110$ °C is shown in Figure 2. Q_{SAXS} starts to increase gradually after a short induction period, increases steeply at $t = t_{H_V}$, and then levels off. The rapid increase after t_{H_V} may suggest a change in the nature of structure development. Note that t_{V_V} and t_{H_V} are the onset times of light scattering invariants Q_{V_V} and Q_{H_V}, respectively.[3] The details of structural development will be discussed by analyzing the SAXS profiles.

The monotonously decreasing profile at stage I suggests that one could apply the Guinier plot for an isolated domain system at very high dilution:[7]

$$I(q,t) \propto \exp[(-R^2/3)q^2] \qquad (2)$$

where R is the radius of gyration, given by $R = (3/5)^{1/2}R_d$ for a spherical domain with radius R_d. Figure 3 shows a typical Guinier plots, showing good straight lines, as

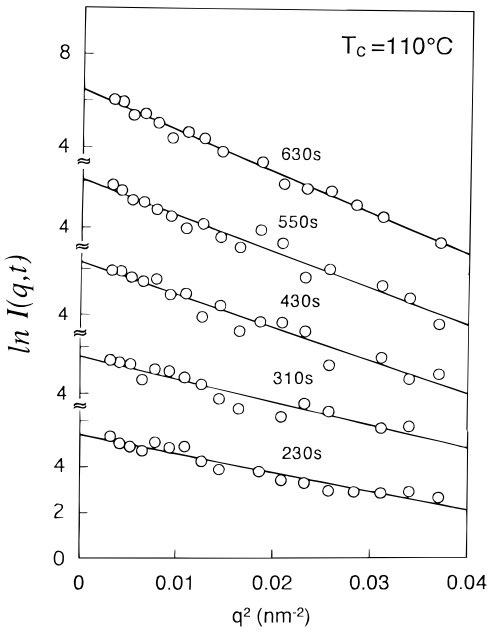

Figure 3. Guinier plots for various crystallization times (stage I).

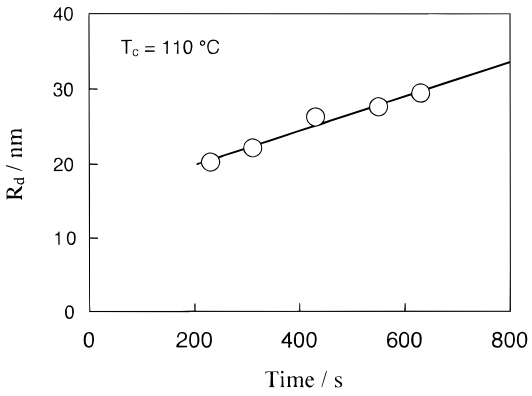

Figure 4. Time variation of the radius of the isolated domain.

expected from eq 2. From the slope of the straight line, one can calculate R_d. The results are shown as a function of crystallization time in Figure 4. The domain of about 20 nm in radius is formed and then grows linearly with time. Regarding the nature of the domain, one could discuss it in the light of structure analysis for stage II, at which the scattering peak appears.

As shown in Figure 1, a peak appears in the SAXS profile at stages II and III. Several variables characterizing the lamellar morphology can be estimated from the correlation function $\gamma_1(r)$, which is given by the Fourier transform of the scattering intensity $I(q)$. The normalized one-dimensional correlation function is given by[6]

$$\gamma_1(r) = \frac{1}{Q_{SAXS}} \int_0^\infty q^2 I(q) \cos(qr)\, dq \qquad (3)$$

where r is the coordinate along which the electron density distribution is measured.

Figure 5 shows a typical example of estimated $\gamma_1(r)$ ($t = 1990$ s, stage II). The long period L can be determined from the position of the first maximum in the correlation function. Another important parameter is the lamellar thickness l_c. The value of l_c may be calculated from the baseline procedure,[8] when the first minimum in correlation function has a flat bottom.

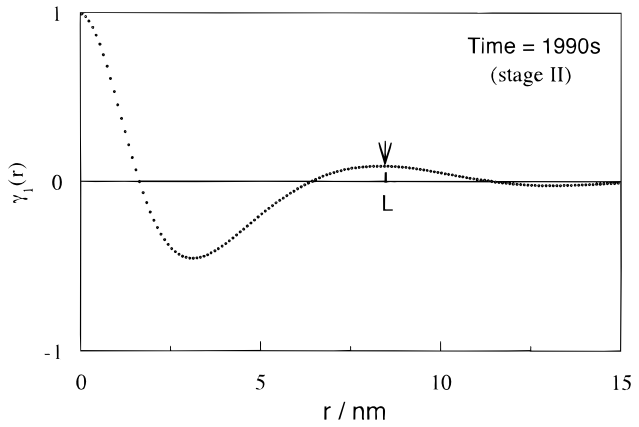

Figure 5. One-dimensional correlation function. Crystallization time = 1990 s (stage II).

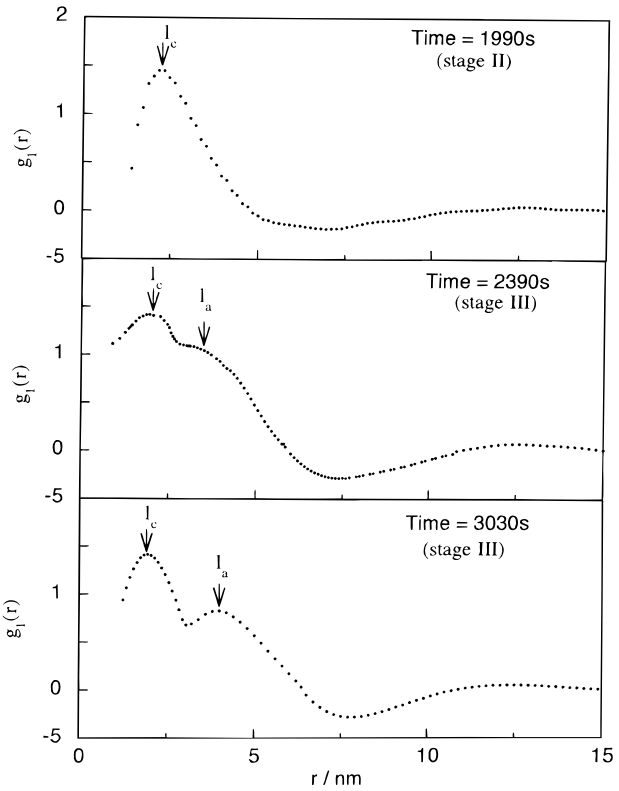

Figure 6. Interface distribution function.

However, the bottom in Figure 5 is not flat (as has been observed in many cases, the nonflat bottom is caused by the broad size distribution of the lamellae). Then, one has to use another method. We employed the interface distribution function $g_1(r)$ method, since this is less affected by the superposition of the maxima or minima caused by the broad distribution than the relevant shape of the correlation function.[9] The function $g_1(r)$ is defined as the second derivative of $\gamma_1(r)$:

$$g_1(r) = \gamma_1(r)'' \tag{4}$$

Figure 6 is the $g_1(r)$ from $\gamma_1(r)$ in Figure 5. A single maximum is seen at stage II. This maximum is ascribed to the crystalline contribution.[10] The l_c is obtained from the position of the first maximum. Note that the estimated lamellar thickness ($l_c \approx 2.3$ nm) is approximately equal to that (2.6 nm) by Groeninckx et al.[11] The second peak is seen at stage III. The absence of the second peak at stage II may be caused by the small

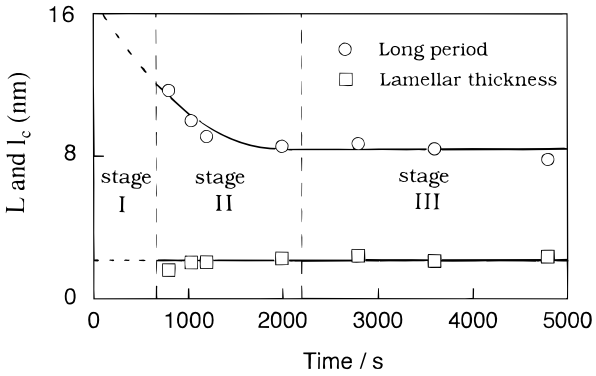

Figure 7. Time variation of the long period L and lamellar thickness l_c.

population of lamellar stacks (small X_L; see later). The time variation of l_c and L is shown in Figure 7. l_c is constant throughout stages II and III, as demonstrated in poly(aryl ether ether ketone).[12] On the other hand, L decreases at stage II and then remains constant at stage III.

If one extrapolates the results in Figure 7 to stage I, at which L and d cannot be experimentally defined, one could discuss the structure at stage I. At stage I, thin lamellae with 2.6 nm thickness are expected to be dispersed in a disordered state in a domain of 20 nm in radius. That is, the lamellar stack has not formed at stage I and several lamellae are arranged irregularly with each other in the domain, as depicted at stage I of Figure 10, in which a line represents a lamella.

At stage II, l_c remains constant, whereas L decreases with time, as shown in Figure 7. It suggests that new lamellae are going to be inserted between the already existing lamellae to establish a lamellar stack. The insertion of lamellae will gradually turn out to be parallel to each other to provide a periodicity which renders SAXS peak.

Combining the SAXS results with the light scattering results in a previous paper,[3] one can estimate the volume fraction of lamellar stacks. Assuming that the amorphous region outside the lamellar stacks does not contribute to Q_{SAXS} at the small angles, one can write[9]

$$Q_{SAXS} = \phi_S X_L X_{CL}(1 - X_{CL})\Delta\rho^2 \tag{5}$$

where ϕ_S is the volume fraction of the spherulite, obtained by light scattering analysis,[3] X_L is the volume fraction of lamellar stacks within the spherulites, X_{CL} is the degree of crystallinity within the lamellar stack, and $\Delta\rho$ ($=\rho_1-\rho_2$) is the difference in the electron density between crystal and amorphous phases.

Using the values of ϕ_S in the previous paper,[3] the values of X_L (arbitrary unit) were calculated. The results are shown as a function of crystallization time in Figure 8. One can see that X_L starts to increase very gradually at stage II, suggesting a slow process for the establishment of the lamellar stacks. Note that, once the stacks are formed, the growth is quite fast (at stage III).

In Figure 9 are summarized the time variations of the various crystalline parameters ranging from nanometers to a few micrometers, obtained from SAXS and light scattering studies. Note that the x-axis of Figure 9 is the radius of the domain at a very early stage (Figure 4; stage I) and, it turns out, the radius of the spherulite at later stages (stages II and III, by light scattering). As shown in Figure 9, V_V light scattering

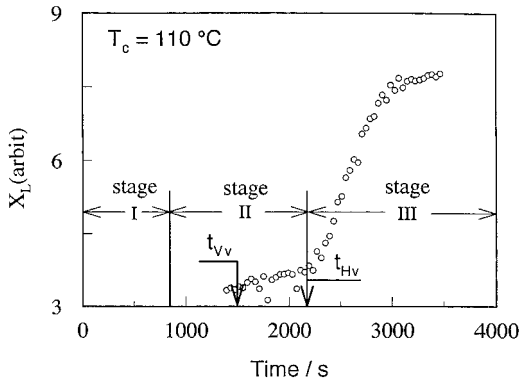

Figure 8. Time variation of the volume fraction of the lamellar stacks.

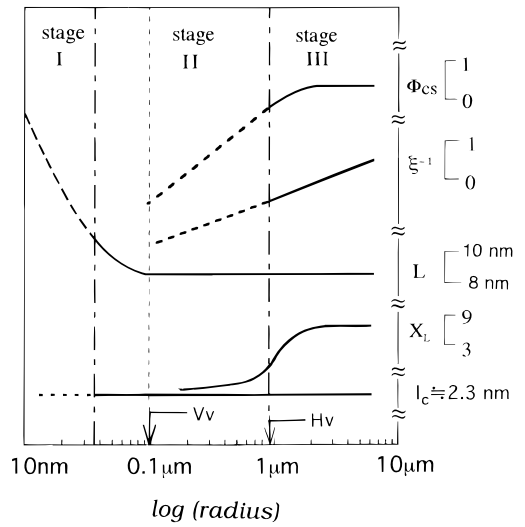

Figure 9. Change in various crystalline parameters with crystallization: the relative crystallinity in spherulite Φ_{cs}, the ordering parameter ξ^{-1}, the volume fraction of the lamellar stacks X_L, the long period L, and the lamellar thickness l_c. The data of Φ_{cs} and ξ^{-1} are reproduced from ref 3.

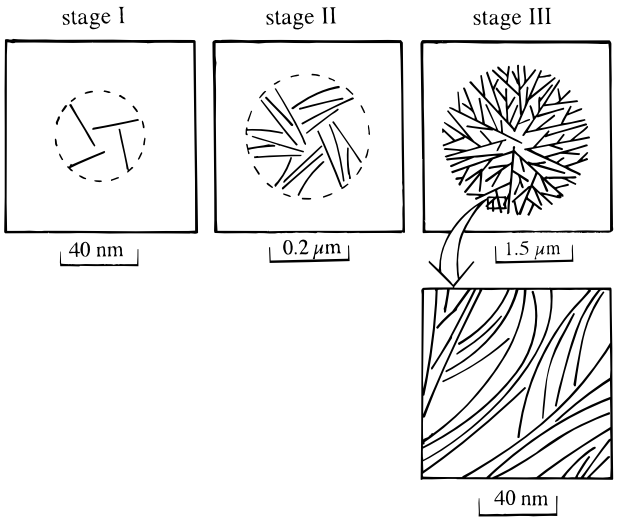

Figure 10. Schematic drawings for the evolution of PET spherulite.

starts to increase at stage II and then H_V light scattering follows at stage III. The time lag ($t_{Vv}-t_{Hv}$) appears at stage II. It suggests that the isotropic domains appear and their internal structure is still too disordered to be detected as a definite H_V scattering. Remembering the argument by SAXS that lamellar stacks develop in stage II, one can conclude that the domain at stage II consists of the highly disordered lamellar stacks, as depicted in stage II of Figure 10.

When stage III starts, the four-leaf-clover pattern characteristic of spherulites is observed in the H_V mode, suggesting that the disordered domain at stage II grows to yield the spherulite with higher ordering, as shown in stage III (top) of Figure 10.[3] The ordering process to yield the spherulite is justified by the time variation of the order parameter, ξ^{-1} (by light scattering).[3] The increase of both X_L and ξ^{-1} implies that the lamellar stacks grow, increasing their mutual ordering. On the other hand, L and l_c are kept constant at stages II and III. It suggests that, once the lamellar stack is established, its internal structure never changes at later stages. The schematic structure in lamellar scale is drawn in stage III (bottom) of Figure 10. The lines in the top and bottom drawings represent the lamellar stacks and lamellae, respectively.

Conclusion

By time-resolved light scattering and time-resolved SAXS using synchrotron radiation, it was shown that the crystallization process of PET consists of three stages as follows. In the early stage, the isolated crystalline domains of several tens of nanometers in diameter, which consist of highly disordered lamellae, appear. Then they develop to yield larger domains of several hundred nanometers in diameter, increasing in size and forming lamellar stacks (stage II). Finally, by increasing the size and volume fraction of the lamellar stacks and keeping the constant long period and lamellae thickness, the isotropic domains grow to a spherulite of about a few micrometers (stage III). The structural development through three stages is schematically depicted in Figure 10.

Acknowledgment. We are thankful for the approval of the Photon Factory Program Advisory Committee in using synchrotron radiation (Proposal 93G246). Also, we are grateful to Dr. Masami Okamoto, Toyobo, Co., Ltd., for a supply of the PET sample and interesting discussion.

References and Notes

(1) Wunderlich, B. *Macromolecular Physics*; Academic Press: New York, 1973; Chapter 3.7.

(2) Norton, B. R.; Keller, A. *Polymer* **1985**, *26*, 704.

(3) Lee, C. H.; Saito, H.; Inoue, T. *Macromolecules* **1993**, *26*, 6566.

(4) Ueki, T.; Hiragi, Y.; Kataoka, M.; Inoko, Y.; Amemiya, Y.; Izumi, T.; Tagawa, H.; Muroga, Y. *Biophys. Chem.* **1985**, *23*, 115.

(5) Koberstein, J. J.; Morra, B.; Stein, R. S. *J. Appl. Crystallogr.* **1980**, *13*, 34.

(6) Glatter, O.; Kratky, O. *Small Angle X-ray Scattering*; Academic Press: London, 1982.

(7) Guinier, A.; Fournet, G. *Small-Angle Scattering of X-Rays*; John Wiley & Sons, Inc.: London, 1955.

(8) Strobl, G. R.; Schneider, M. T.; Voigt-Martin, I. G. *J. Polym. Sci., Polym. Phys. Ed.* **1980**, *18*, 1361.

(9) Santa Cruz, C.; Stribeck, N.; Zachmann, H. G.; Balta Calleja, F. J. *Macromolecules* **1991**, *24*, 5980.

(10) Albrecht, T.; Strobl, G. R. *Macromolecules* **1996**, *29*, 783.

(11) Groeninckx, G.; Reynaers, H.; Berghmans, H.; Smets, G. *J. Polym. Sci., Polym. Phys. Ed.* **1980**, *18*, 1311.

(12) Hsiao, B. S.; Gardner, K. H.; Wu, D. Q.; Chu, B. *Polymer* **1993**, *34*, 3986.

MA951828M